JOURNAL OF COMPUTATIONAL PHYSICS **133,** 323–339 (1997)
ARTICLE NO. CP975671

A Fast Iterative Method for Computing Particle Beams Penetrating Matter

Christoph Börgers

Department of Mathematics, Tufts University, Medford, Massachusetts 02155

Received July 18, 1996; revised February 4, 1997

Beams of microscopic particles penetrating matter are important in several fields. The application motivating our parameter choices in this paper is electron beam cancer therapy. Mathematically, a steady particle beam penetrating matter, or a configuration of several such beams, is modeled by a boundary value problem for a Boltzmann equation. Grid-based discretization of this problem leads to a system of algebraic equations. This system is typically very large because of the large number of independent variables in the Boltzmann equation (six if time independence is the only dimension-reducing assumption). If grid-based methods are to be practical at all, it is therefore necessary to develop fast solvers for the discretized problems. This is the subject of the present paper. For two-dimensional, mono-energetic, linear particle beam problems, we describe an iterative domain decomposition algorithm based on overlapping decompositions of the set of particle directions and computationally demonstrate its rapid, grid independent convergence. There appears to be no fundamental obstacle to generalizing the method to three-dimensional, energy dependent problems.

1. INTRODUCTION

Particle beams penetrating matter are of interest in several fields. The example motivating our parameter choices in this paper is electron beam cancer therapy; for an introductory book on this subject, see for instance [17]. Other examples are electron microscopy [29], and ion beams used to modify the properties of materials [34].

Mathematically, a steady particle beam, or a configuration of several such beams, is modeled by a boundary value problem for a Boltzmann equation. This equation is linear or nonlinear depending on whether the beam particles don't or do interact with each other. We will assume linearity. This is a common assumption in electron beam therapy planning. The dependent variable in the Boltzmann equation is the *phase space density*, i.e., the number of particles per unit volume in position–velocity space. This is in general a function of position, velocity, and time. In many applications, including electron beam therapy, the main interest is in time independent problems. There are then six independent variables, three position and three velocity coordinates. As a result of this large number of independent variables, grid-based discretization of a boundary value problem for a Boltzmann equation leads to a very large system of algebraic equations. If grid-based methods are to be practical at all, it is necessary to develop fast solvers for the discretized problems. This is the subject of the present paper.

We make the following two assumptions. First, scattering of beam particles by the background is frequent and *forward-peaked*; i.e., the deflection experienced by a beam particle in a single collision with a background particle is likely to be small. Second, the total direction change experienced by a beam particle between entering and leaving the background material is likely to be moderate.

The limit of infinitely frequent, infinitesimally weak (that is, forward-peaked) collisions is called the *Fokker–Planck limit*; see Section 3. Thus our first assumption means that we consider problems near the Fokker–Planck limit. In this limit, the linear Boltzmann equation becomes the *Fokker–Planck equation*. In the medical physics literature, an approximation to the Fokker–Planck equation, called the *Fermi equation*, is often used; see [30, 14], and Eq. (25) below. This approximation is accurate for a mono-directional beam normally incident on a homogeneous slab as long as beam broadening due to particle–background collisions is moderate. In fact, the Fermi equation can be viewed as the leading term in an asymptotic expansion of the Fokker–Planck equation, the small parameter being the amount of beam broadening per unit penetration depth; see [21, 1]. Thus our second assumption means that we consider problems near the *Fermi limit*. Our numerical results show that in fact we need not be very close to either limit for our method to be rapidly convergent.

Our main point in this paper is that near the Fokker–Planck and Fermi limits, *angular domain decomposition*, i.e., domain decomposition based on decompositions of the set of particle directions, is a natural and effective approach to solving the discrete problem. We present an algorithm of this kind for a model problem, mono-energetic linear particle transport in two space dimensions, and demonstrate its effectiveness through numerical experiments.

0021-9991/97 $25.00

We emphasize that our model problem is not, strictly speaking, a physical one. It is different from, and simpler than, the orthogonal projection into a plane of mono-energetic transport in three space dimensions. If all particles move at a constant speed c, transport in two space dimensions involves velocity vectors of length c only, while the orthogonal projection into a plane of transport in three space dimensions involves two-dimensional velocity vectors of any length between 0 and c.

In Sections 2 and 3, we present the equations governing mono-energetic linear particle transport in two space dimensions. In Sections 4 and 5 we discuss choices of the scattering law and the parameters in the equation that make our model problem reminiscent of the electron beam therapy problem. Our iterative algorithm for the Fokker–Planck equation is described at the continuous level, i.e., without reference to any discretization, in Section 6. An analogous algorithm for the heat equation in one space dimension is described and analyzed in Section 7. We see no reason to use this algorithm for the heat equation, but its analysis clarifies why and how the method of Section 6 works. In Section 8, we present two variations of the algorithm of Section 6 for the linear Boltzmann equation. The first is not easily parallelizable; the second is, at the expense of a slight loss in convergence speed. Our computational results are reported in Sections 9 and 10. In Section 11, we discuss possible extensions and limitations of our approach, and its relation to some other methods for solving particle transport problems with forward-peaked scattering proposed in the literature.

2. MONO-ENERGETIC LINEAR PARTICLE TRANSPORT IN TWO SPACE DIMENSIONS

In this section, we mix mathematical and physical terminology; it will always be obvious how the more intuitive physical terminology could be translated into strictly mathematical language. We discuss mono-energetic transport in two space dimensions. As mentioned in the introduction, this is simpler than the more familiar orthogonal projection into a plane of mono-energetic transport in three space dimensions.

We consider the motion of particles in a domain $\Omega \subseteq \mathbb{R}^2$. All particles move at the same constant speed $c > 0$. Each particle experiences collisions at random times, causing random directional changes. The inter-collision distances $\lambda > 0$ (Fig. 1) are random and independent of each other, with exponential distribution; their expectation $\overline{\lambda} > 0$ is called the *mean free path*. The deflection angles η (Fig. 1) are random, independent of each other, with probability density function p: $(-\pi, \pi) \to \mathbb{R}_+$. We assume p to be even. Violation of this assumption is physically unreasonable—a particle ought to have no preference for scattering to the right over scattering to the left or vice versa. An example of p is shown in Fig. 2. The forward-peakedness of the scattering translates into a sharp peak in the graph of p near $\eta = 0$; in reality, the peak would typically be very much more pronounced than in Fig. 2.

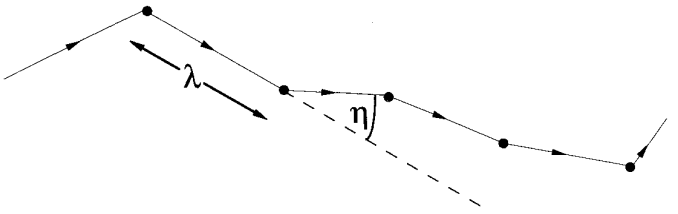

FIG. 1. Path of a particle, with intercollision distance λ and deflection angle η.

The *phase space density* $f = f(\mathbf{x}, \mathbf{u}, t)$ is the number of particles per unit $(\mathbf{x}, \mathbf{u})$-volume, where $\mathbf{x} = (x, y) \in \Omega$ denotes the particle position, $\mathbf{u} = (u, v) \in S^1$ the particle direction, and $t \geq 0$ time. We use the notation

$$\mathbf{u} = (u, v) = (\cos\theta, \sin\theta), \theta \in \mathbb{R},$$

and often identify functions of $\mathbf{u} \in S^1$ with 2π-periodic functions of $\theta \in \mathbb{R}$.

The time evolution of f is governed by the *linear Boltzmann equation*, the mathematical statement of the law of conservation of particles,

$$f_t + cuf_x + cvf_y = cQf, \tag{1}$$

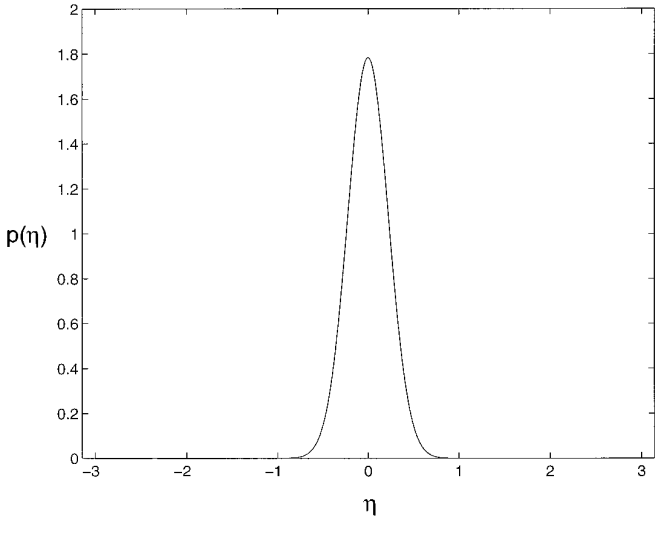

FIG. 2. Probability density function of deflection angle η.

where the *collision operator* Q is defined by

$$Qf = \frac{1}{\lambda}(p * f - f),$$

and $*$ denotes convolution with respect to θ:

$$(p * f)(\theta) = \int_{-\pi}^{\pi} p(\eta) f(\theta - \eta)\, d\eta. \tag{2}$$

Here, as several times later in this paper, we have simplified the notation by omitting the arguments $\mathbf{x}$ and t. The derivation of Eq. (1) from the law of conservation of particles is easy and standard; see for instance [6] for the derivation of the analogous equation in three space dimensions.

To prepare the use of Fourier expansions in later sections, we introduce the notation

$$c_n = \int_{-\pi}^{\pi} \exp(-in\eta) p(\eta)\, d\eta \tag{3}$$

and

$$\hat{f}_n = \frac{1}{2\pi} \int_{-\pi}^{\pi} \exp(-in\theta) f(\theta)\, d\theta \tag{4}$$

for integers n. Notice that a factor of $1/(2\pi)$ is included in Eq. (4), but not in Eq. (3); this will lead to minor notational simplifications. We note that

$$c_n = \int_{-\pi}^{\pi} \cos(n\eta) p(\eta)\, d\eta$$

because of our assumption that p is even. Thus c_n is real, $c_n = c_{-n}$, $c_0 = 1$, and $c_n \in (-1, 1)$ for $n \neq 0$.

Since convolution of functions corresponds to multiplication of their Fourier coefficients, we obtain the following representation of the collision operator:

$$Qf(\theta) = \frac{1}{\lambda}(p * f - f)(\theta) = \sum_n \frac{c_n - 1}{\lambda} \hat{f}_n \exp(in\theta). \tag{5}$$

As mentioned before, the problems arising in applications are often time independent. We will assume time independence from now on. For our model problem, this means that $f = f(\mathbf{x}, \mathbf{u})$. The problems of interest are of the form

$$(uf_x + vf_y)(\mathbf{x}, \mathbf{u}) = Qf(\mathbf{x}, \mathbf{u}) \quad \text{for } (\mathbf{x}, \mathbf{u}) \in \Omega \times S^1, \tag{6}$$

$$f(\mathbf{x}, \mathbf{u}) = g(\mathbf{x}, \mathbf{u}) \quad \text{for } (\mathbf{x}, \mathbf{u}) \in \partial^- \Omega, \tag{7}$$

with g given and

$$\partial^- \Omega = \{(\mathbf{x}, \mathbf{u}) \in \partial\Omega \times S^1 : \mathbf{u} \cdot \mathbf{n}(\mathbf{x}) < 0\},$$

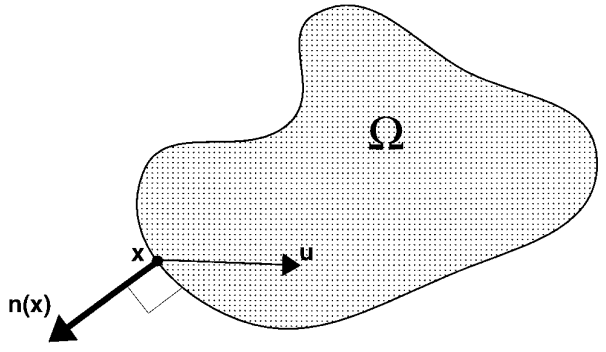

FIG. 3. Spatial domain Ω, exterior unit normal vector $\mathbf{n}$, inflow direction $\mathbf{u}$.

where $\mathbf{n}$ denotes the exterior unit normal vector field on $\partial\Omega$; see Fig. 3.

3. THE FOKKER–PLANCK LIMIT

In this section, we present a two-dimensional version of some of the material in the Appendix of [2], which in turn was a specialized but more precise version of some of the discussion in [27].

In the Fokker–Planck limit, collisions become infinitely frequent and infinitesimally weak (that is, forward-peaked), in such a way that the two effects balance each other; the precise meaning of this statement will become clear in this section. When collisions are strongly forward-peaked, i.e., when $p(\eta)$ is small everywhere except near $\eta = 0$, the following calculation is plausible:

$$\begin{aligned}\frac{1}{\lambda}(p * f - f)(\theta) &= \frac{1}{\lambda}\left(\int_{-\pi}^{\pi} p(\eta) f(\theta - \eta)\, d\eta - f(\theta)\right) \\ &\approx \frac{1}{\lambda}\left(\int_{-\pi}^{\pi} p(\eta)\left(f(\theta) - f_\theta(\theta)\eta + f_{\theta\theta}(\theta)\frac{\eta^2}{2}\right) d\eta - f(\theta)\right) \\ &= D f_{\theta\theta}(\theta),\end{aligned}$$

where the *angular diffusion coefficient* D is defined by

$$D = \frac{1}{2\lambda} \int_{-\pi}^{\pi} \eta^2 p(\eta)\, d\eta. \tag{8}$$

In this calculation, we have used $\int_{-\pi}^{\pi} p(\eta)\, d\eta = 1$ and $\int_{-\pi}^{\pi} \eta p(\eta)\, d\eta = 0$; the latter follows from the assumption that p is even. We note that D is the reciprocal of a length. We introduce the notation

$$Q_{\mathrm{FP}} = D \frac{\partial^2}{\partial \theta^2}.$$

The equation

$$uf_x + vf_y = Q_{\mathrm{FP}} f \tag{9}$$

is called the Fokker–Planck equation.

We next state and prove a proposition clarifying when and in which sense the above calculation is valid. First we introduce some notation. We write

$$H^2_{\mathrm{per}} = \Big\{ f : \mathbb{R} \to \mathbb{R} \,|\, f \text{ is periodic with period } 2\pi, \text{ and } \int_0^{2\pi} (f_{\theta\theta}(\theta))^2 \, d\theta < \infty \Big\}.$$

For $f \in H^2_{\mathrm{per}}$ and $p \in L^2(-\pi, \pi)$, the convolution $p * f$, defined in Eq. (2), belongs to H^2_{per}. Sometimes we think of functions in H^2_{per} as elements of $L^2(0, 2\pi)$; i.e., we identify $f \in H^2_{\mathrm{per}}$ with its restriction to the interval $(0, 2\pi)$. It will be clear from the context when we make this identification. We denote weak convergence in $L^2(0, 2\pi)$ by "$\rightharpoonup$".

PROPOSITION 1. *For $k = 1, 2, 3, \ldots$, let $\overline{\lambda}_k > 0$ be numbers and let $p_k \in L^2(-\pi, \pi)$ be even probability densities, with*

$$\lim_{k\to\infty} \overline{\lambda}_k = 0, \tag{10}$$

$$\lim_{k\to\infty} \int_{-\pi}^{\pi} \eta^2 p_k(\eta) \, d\eta = 0, \tag{11}$$

$$\textit{and} \quad \lim_{k\to\infty} \frac{\int_{-\pi}^{\pi} \eta^2 p_k(\eta) \, d\eta}{2\overline{\lambda}_k} = D > 0. \tag{12}$$

Then

$$\frac{p_k * f - f}{\overline{\lambda}} \rightharpoonup D f_{\theta\theta}$$

for all $f \in H^2_{\mathrm{per}}$ if and only if

$$\lim_{k\to\infty} \frac{\int_{-\pi}^{\pi} \eta^4 p_k(\eta) \, d\eta}{\int_{-\pi}^{\pi} \eta^2 p_k(\eta) \, d\eta} = 0. \tag{13}$$

Proof. Since weak convergence in $L^2(0, 2\pi)$ means the same as convergence of all Fourier coefficients, we must show that Eq. (13) is equivalent to

$$\lim_{k\to\infty} \frac{c_{k,n} - 1}{\overline{\lambda}_k} = -n^2 D \quad \text{for all } n, \tag{14}$$

where

$$c_{k,n} = \int_{-\pi}^{\pi} \exp(-in\eta) p_k(\eta) \, d\eta.$$

By Taylor's theorem,

$$\frac{c_{k,n} - 1}{\overline{\lambda}_k} = \frac{1}{\overline{\lambda}_k} \left(\int_{-\pi}^{\pi} \exp(-in\eta) p_k(\eta) \, d\eta - 1 \right) = \frac{1}{\overline{\lambda}_k} \left(\int_{-\pi}^{\pi} \left(1 - \frac{n^2\eta^2}{2} + \frac{n^4\eta^4\vartheta^4}{24} \right) p_k(\eta) \, d\eta - 1 \right),$$

for some ϑ between 0 and 1. Thus

$$\frac{c_{k,n} - 1}{\overline{\lambda}_k} = -n^2 \frac{\int_{-\pi}^{\pi} \eta^2 p_k(\eta) \, d\eta}{2\overline{\lambda}_k} + E_{k,n},$$

with

$$E_{k,n} = \frac{n^4}{24\overline{\lambda}_k} \int_{-\pi}^{\pi} \vartheta^4 \eta^4 p_k(\eta) \, d\eta.$$

This shows that Eqs. (12) and (13) imply Eq. (14). Conversely, assume Eq. (14). In fact, we need (14) with $n = 1$ only:

$$\begin{aligned}
&\lim_{k\to\infty} \frac{c_{k,1} - 1}{\overline{\lambda}_k} = -D \\
\Leftrightarrow &\lim_{k\to\infty} \frac{1}{\overline{\lambda}_k} \int_{-\pi}^{\pi} (\exp(-i\eta) - 1) p_k(\eta) \, d\eta = -D \\
\Leftrightarrow &\lim_{k\to\infty} \frac{1}{\overline{\lambda}_k} \int_{-\pi}^{\pi} \left(\exp(-i\eta) - 1 + \frac{\eta^2}{2} \right) p_k(\eta) \, d\eta = 0 \qquad (15) \\
\Leftrightarrow &\lim_{k\to\infty} \frac{\int_{-\pi}^{\pi} (\exp(-i\eta) - 1 + \eta^2/2) p_k(\eta) \, d\eta}{\int_{-\pi}^{\pi} \eta^2 p_k(\eta) \, d\eta} = 0 \\
\Leftrightarrow &\lim_{k\to\infty} \frac{\int_{-\pi}^{\pi} (\cos\eta - 1 + \eta^2/2) p_k(\eta) \, d\eta}{\int_{-\pi}^{\pi} \eta^2 p_k(\eta) \, d\eta} = 0.
\end{aligned}$$

Since

$$\min_{0<|\eta|\le\pi} \frac{\cos\eta - 1 + \eta^2/2}{\eta^4} = \frac{\pi^2 - 4}{2\pi^4} > 0,$$

Eq. (15) implies Eq. (13), completing the proof of our proposition. ∎

Eq. (10) expresses that collisions become infinitely frequent, Eq. (11) expresses that they become infinitesimally weak, and Eq. (12) makes precise what it means for the two effects to balance each other. The Fokker–Planck approximation to Eqs. (6) and (7) is

$$(uf_x + vf_y)(\mathbf{x}, \mathbf{u}) = Q_{\mathrm{FP}} f(\mathbf{x}, \mathbf{u}) \quad \text{for } (\mathbf{x}, \mathbf{u}) \in \Omega \times S^1, \tag{16}$$

$$f(\mathbf{x}, \mathbf{u}) = g(\mathbf{x}, \mathbf{u}) \quad \text{for } (\mathbf{x}, \mathbf{u}) \in \partial^- \Omega. \tag{17}$$

4. EXAMPLES OF INTEGRAL COLLISION OPERATORS

In this section, we consider a family of examples of probability densities p on $(-\pi, \pi)$. We then choose a subfamily making our problem reminiscent of the scattering of electrons by background nuclei.

For $\varepsilon > 0$, $q \geq 0$, and $\eta \in (-\pi, \pi)$, we define

$$p(\varepsilon, q; \eta) = \frac{C(\varepsilon, q)}{(2(1 - \cos \eta) + \varepsilon^2)^{q/2}},$$

where $C(\varepsilon, q)$ is the constant needed to make the integral of p equal to 1:

$$C(\varepsilon, q) = \left[\int_{-\pi}^{\pi} \frac{1}{(2(1 - \cos \eta) + \varepsilon^2)^{q/2}} \, d\eta \right]^{-1},$$

This is less arbitrary than it may seem: For $\varepsilon \ll |\eta| \ll 1$, p is approximately proportional to $1/\eta^q$. Our definition of p represents a simple way of correcting two deficiencies that the more straightforward choice $p \sim 1/\eta^q$ would have, its singularity at $\eta = 0$ and its lack of periodicity.

Our next proposition shows that in the limit as $\varepsilon \to 0$, the collisions become infinitesimally weak if and only if $q \geq 1$, and the Fokker–Planck approximation is valid if and only if $q \geq 3$:

PROPOSITION 2. *As $\varepsilon \to 0$ with q fixed,*

$$\int_{-\pi}^{\pi} \eta^2 p(\varepsilon, q; \eta) \, d\eta = \begin{cases} O(1) & \text{if } 0 \leq q < 1, \\ O(1/\ln(1/\varepsilon)) & \text{if } q = 1, \\ O(\varepsilon^{q-1}) & \text{if } 1 < q < 3, \\ O(\varepsilon^2 \ln(1/\varepsilon)) & \text{if } q = 3, \\ O(\varepsilon^2) & \text{if } q > 3, \end{cases}$$

and

$$\frac{\int_{-\pi}^{\pi} \eta^4 p(\varepsilon, q; \eta) \, d\eta}{\int_{-\pi}^{\pi} \eta^2 p(\varepsilon, q; \eta) \, d\eta} = \begin{cases} O(1) & \text{if } 0 \leq q < 3, \\ O(1/\ln(1/\varepsilon)) & \text{if } q = 3, \\ O(\varepsilon^{q-3}) & \text{if } 3 < q < 5, \\ O(\varepsilon^2 \ln(1/\varepsilon)) & \text{if } q = 5, \\ O(\varepsilon^2) & \text{if } q > 5. \end{cases}$$

Proof. Define

$$\tilde{p}(\varepsilon, q; \eta) = \frac{\tilde{C}(\varepsilon, q)}{(\eta^2 - \varepsilon^2)^{q/2}},$$

with

$$\tilde{C}(\varepsilon, q) = \left[\int_{-\pi}^{\pi} \frac{1}{(\eta^2 + \varepsilon^2)^{q/2}} \, d\eta \right]^{-1}.$$

Since

$$\frac{4}{\pi^2} \eta^2 \leq 2(1 - \cos \eta) \leq \eta^2$$

for all $\eta \in [-\pi, \pi]$, it is enough to prove our assertions with p replaced by $\tilde{p}$.

Straightforward calculations yield

$$\tilde{C}(\varepsilon, q) = \begin{cases} O(1) & \text{if } 0 \leq q < 1, \\ O(1/\ln(1/\varepsilon)) & \text{if } q = 1, \\ O(\varepsilon^{q-1}) & \text{if } q > 1, \end{cases} \tag{18}$$

$$\int_{-\pi}^{\pi} \frac{\eta^2}{(\eta^2 + \varepsilon^2)^{q/2}} \, d\eta = \begin{cases} O(1) & \text{if } 0 \leq q < 3, \\ O(\ln(1/\varepsilon)) & \text{if } q = 3, \\ O(\varepsilon^{3-q}) & \text{if } q > 3, \end{cases} \tag{19}$$

and

$$\int_{-\pi}^{\pi} \frac{\eta^4}{(\eta^2 + \varepsilon^2)^{q/2}} \, d\eta = \begin{cases} O(1) & \text{if } 0 \leq q < 5, \\ O(\ln(1/\varepsilon)) & \text{if } q = 5, \\ O(\varepsilon^{5-q}) & \text{if } q > 5, \end{cases} \tag{20}$$

(The reason for replacing p by $\tilde{p}$ is that Eqs. (18)–(20) can be obtained by explicit calculation.) Our assertions are obtained by combining Eqs. (18)–(20). ∎

The most interesting special case is $q = 3$:

$$p(\varepsilon; \eta) = \frac{C(\varepsilon)}{(2(1 - \cos \eta) + \varepsilon^2)^{3/2}}. \tag{21}$$

Proposition 2 shows that with this choice of p, the collisions become infinitesimally weak as $\varepsilon \to 0$, and the Fokker–Planck approximation is valid, but just barely—the ratio of the fourth and second moments tends to zero logarithmically. In three dimensions, the *screened Rutherford scattering cross section* [33], the simplest physically realistic model of the scattering of electrons by nuclei, has the precisely analogous properties [2]. Therefore we call (21) the *screened Rutherford scattering law in two space dimensions*.

We will also use $q = 2$ as a test case:

$$p(\varepsilon; \eta) = \frac{C(\varepsilon)}{2(1 - \cos \eta) + \varepsilon^2}. \tag{22}$$

Proposition 2 shows that with this choice of p, the collisions also become infinitesimally weak as $\varepsilon \to 0$, but the Fokker–Planck approximation is invalid. (In fact it is not hard to show that in the limit $\varepsilon \to 0$, one obtains an operator proportional to $-\sqrt{-\partial^2/\partial\theta^2}$ rather than $\partial^2/\partial\theta^2$.) The notation becomes simpler here if the parameter ε is replaced by

$$g = 1 + \frac{\varepsilon^2}{2} - \sqrt{\varepsilon^2 + \frac{\varepsilon^4}{4}}.$$

Notice that $\varepsilon \to 0$ is equivalent to $g \to 1$. With this notation, Eq. (22) becomes

$$p(g; \eta) = \frac{C(g)}{1 - 2g\cos\eta + g^2},$$

where $C(g)$ is again the constant needed to make the integral equal to 1. It is a straightforward calculation to check that $C(g) = (1 - g^2)/(2\pi)$, so

$$p(g; \eta) = \frac{1}{2\pi}\frac{1 - g^2}{1 - 2g\cos\eta + g^2}. \tag{23}$$

The Fourier expansion of p is particularly simple: For $|g| < 1$ and $\eta \in \mathbb{R}$,

$$p(g; \eta) = \frac{1}{2\pi}\sum_{n=-\infty}^{\infty} g^{|n|}\exp(in\eta), \tag{24}$$

which follows from the formula for the sum of a geometric series. In three dimensions, the Henyey–Greenstein scattering kernel [9] has very similar properties [27]; in particular, Eq. (24) is the analog of Eq. (59) of [27]. We therefore call (23) the *Henyey–Greenstein scattering law in two space dimensions*. It is of interest to us only as an example demonstrating that our method works well in at least some cases in which approximation of the collision operator Q by the Fokker–Planck operator Q_{FP} is invalid.

5. REALISTIC PARAMETER VALUES

In this section, we discuss how to choose the mean free path $\overline{\lambda}$ and the angular diffusion coefficient D in order to make our model problem reminiscent of the problems in electron beam radiation therapy planning. We begin by considering a beam of particles normally incident on the strip $\Omega = (0, L) \times \mathbb{R}$, as shown in Fig. 4. All particles move in directions $(\cos\theta, \sin\theta)$ with $\theta \approx 0$. If we therefore approximate $u = \cos\theta$ by 1 and $v = \sin\theta$ by θ in the Fokker–Planck equation (9), we obtain

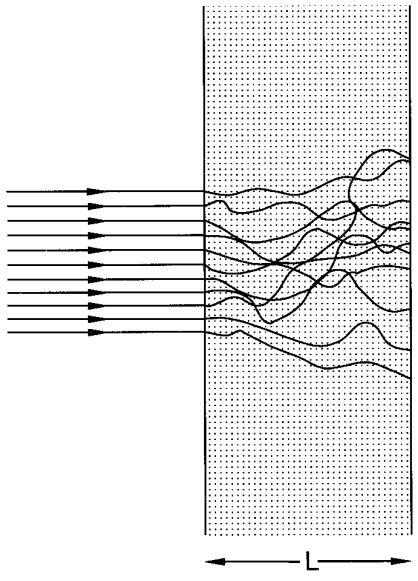

FIG. 4. Particles normally incident on a scattering slab.

$$f_x + \theta f_y = D f_{\theta\theta}. \tag{25}$$

In the medical physics literature, the three-dimensional analog of this equation is called the Fermi equation; see [30, 14].

We introduce dimensionless variables to eliminate the parameters L and D:

$$\hat{x} = \frac{x}{L}, \quad \hat{y} = \frac{y}{(DL)^{1/2}L}, \quad \hat{\theta} = \frac{\theta}{(DL)^{1/2}}.$$

Equation (25) then becomes

$$f_{\hat{x}} + \hat{\theta} f_{\hat{y}} = f_{\hat{\theta}\hat{\theta}},$$

and the transformed spatial domain is $\hat{\Omega} = (0, 1) \times \mathbb{R}$. This shows that the amount by which the beam broadens as it penetrates the strip of depth L is $\approx (DL)^{1/2} L$. For the beam to remain recognizable as a beam, $(DL)^{1/2} L$ should be $\ll L$. Thus we conclude that in beam problems,

$$(DL)^{1/2} \ll 1,$$

where L denotes the penetration depth of interest. The method described in this paper converges rapidly when $DL < 1$. Thus it is effective for beam problems.

TABLE I

Angular Diffusion Coefficient D as a Function of Energy E_0 of Entering Beam, from [12]

E_0 [MeV]	D [cm^{-1}]
5	0.0583
8	0.0259
10	0.0175
15	0.00848
20	0.00505
30	0.00240

Specific values of D for electrons passing through various background materials can be derived for instance from [10] or from [12, p. 134, Table I]. To see how the notation translates, compare our Eq. (25) with Eqs. (9) and (128) in [12]:

$$D = \frac{\rho}{4} \times \frac{k_0}{\rho},$$

where ρ is the background density and k_0/ρ is the quantity tabulated, as a function of initial energy E_0, on p. 134 of [12]. For water, using $\rho = 1$ g/cm^3, we find the values of D summarized in Table I. If L is a few centimeters (an electron beam of initial energy E_0 in water approximately reaches the depth $E_0/2$ cm/MeV, compare for instance [17, p. 395, Fig. 6.13]), we see that realistic values of DL are around 0.1 or less.

Mean free paths of electrons passing through water can be computed from [26]. The elastic collision cross section for electron-hydrogen interactions is approximately 13,000 bn, and that for electron–oxygen interactions is approximately 210,000 bn; see [26, pp. 3, 32]. Therefore the total cross section for elastic collisions of electrons in water is approximately $2 \times 13{,}000 + 210{,}000$ bn $= 236{,}000$ bn. Denoting Avogadro's number by N_A, the number of elastic collisions per centimeter is approximately

$$\frac{1\text{ g}}{\text{cm}^3} \times \frac{N_A}{g} \times \frac{1}{18} \times \text{elastic collision cross section in cm}^2 \times 1\text{ cm} \approx 8{,}000.$$

Again considering a penetration depth of a few centimeters, we see that realistic values of $L/\bar{\lambda}$ are a few tens of thousands.

6. THE ITERATION FOR THE FOKKER–PLANCK EQUATION

The method for Eqs. (16) and (17) proposed in this section is a Schwarz type iterative domain decomposition algorithm. The literature on such algorithms, especially for elliptic boundary value problems, is extensive; see for instance the proceedings [18, 28]. However, to our knowledge the method described here has not been suggested before.

Let $\hat{I}$ be an open interval of length smaller than π, and denote by I the corresponding subset of S^1:

$$I = \{(\cos\theta, \sin\theta) \in S^1 : \theta \in \hat{I}\}.$$

If $\mathbf{u}$ is restricted to I, the Fokker–Planck equation can be viewed as a "time"-dependent convection–diffusion equation. In this equation, the role of time is played by the direction of the vector $(\cos\theta_0, \sin\theta_0)$ in the (x, y)-plane, where θ_0 is the midpoint of $\hat{I}$, the direction of $(\sin\theta_0, -\cos\theta_0)$ is the convection direction, and the θ-direction is the diffusion direction. To explain this, take the example $\hat{I} = (-\pi/4, \pi/4)$. For $\theta \in (-\pi/4, \pi/4)$, the Fokker–Planck equation can be written in the form

$$f_x + \tan\theta\, f_y = \frac{D}{\cos\theta} f_{\theta\theta}. \tag{26}$$

(Notice that $\cos\theta > 1/\sqrt{2}$ for $\theta \in (-\pi/4, \pi/4)$.) Equation (26) is a convection–diffusion equation in which the x-direction plays the role of time, the convection is in the y-direction, and the diffusion is in the θ-direction. As a second example, consider $\hat{I} = (0, \pi/2)$. For $\theta \in (0, \pi/2)$, the Fokker–Planck equation can be written in the form

$$\frac{f_x + f_y}{\sqrt{2}} + \frac{\cos\theta - \sin\theta}{\cos\theta + \sin\theta} \frac{f_x - f_y}{\sqrt{2}} = \frac{\sqrt{2}}{\cos\theta + \sin\theta} D f_{\theta\theta}. \tag{27}$$

(Notice that $\cos\theta + \sin\theta > 1$ for $\theta \in (0, \pi/2)$.) Equation (27) is a convection–diffusion equation in which the direction of the unit vector $(1, 1)/\sqrt{2}$ in the (x, y)-plane plays the role of time, the convection is in the direction of the unit vector $(1, -1)/\sqrt{2}$ in the (x, y)-plane, and the diffusion is in the θ-direction.

For $\nu = 1, 2, 3, 4$, we introduce the notation

$$\mathbf{a}_\nu = (\cos(\nu\pi/2 - \pi/4), \sin(\nu\pi/2 - \pi/4)) \quad \text{and}$$

$$\mathbf{b}_\nu = (\cos(\nu\pi/2), \sin(\nu\pi/2));$$

compare Fig. 5. If $f(\mathbf{x}, \mathbf{a}_\nu)$ were given for $\nu = 1, 2, 3, 4$, then all of f could be computed inexpensively using the observation above by solving four convection–diffusion problems, with $\hat{I}$ equal to $(-\pi/4, \pi/4)$, $(\pi/4, 3\pi/4)$, $(3\pi/4, 5\pi/4)$, and $(5\pi/4, 7\pi/4)$. Similarly, if $f(\mathbf{x}, \mathbf{b}_\nu)$ were given for $\nu = 1, 2, 3, 4$, then all of f could be computed inexpensively by solving four convection–diffusion problems, with $\hat{I}$ equal to $(0, \pi/2)$, $(\pi/2, \pi)$, $(\pi, 3\pi/2)$, and $(3\pi/2, 2\pi)$. This leads to our iterative algorithm:

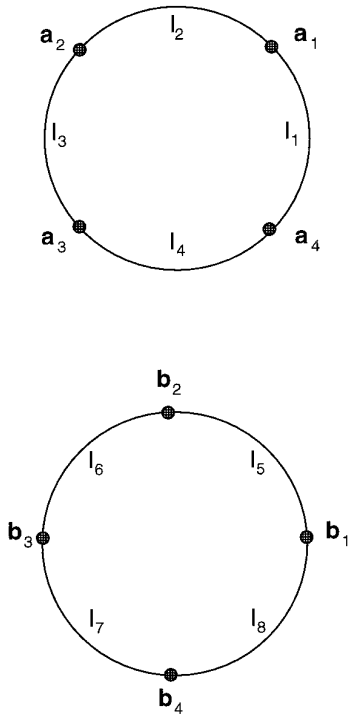

FIG. 5. Two decompositions of S^1.

1. Given approximations for $f(\mathbf{x}, \mathbf{a}_\nu)$, $\mathbf{x} \in \Omega$, $\nu = 1, 2, 3, 4$, compute an approximation for all of f by solving four convection-diffusion equations. In particular, this yields approximations for $f(\mathbf{x}, \mathbf{b}_\nu)$, $\mathbf{x} \in \Omega$, $\nu = 1, 2, 3, 4$.

2. Based on these approximations, compute a new approximation for all of f, again by solving four convection–diffusion problems. In particular, this yields new approximations for $f(\mathbf{x}, \mathbf{a}_\nu)$, $\mathbf{x} \in \Omega$, $\nu = 1, 2, 3, 4$.

Iterate this process.

The four convection–diffusion problems in the first step can be solved in parallel, independent of each other, and the same holds for the second step.

7. ANALYSIS OF A SIMILAR ITERATION FOR THE HEAT EQUATION

We next describe and analyze an iterative method analogous to that of Section 6 for the heat equation in one space dimension. We do not propose this method as a good way of solving the heat equation, but present it because its analysis casts light on why and how the method of Section 6 works. A similar analysis could likely be carried out for the method of Section 6 itself, but would be more technical and less explicit.

The notation for the independent variables used in this section is unusual in the context of the heat equation, but helps clarify the analogy with the Fokker–Planck equation. We consider the problem of finding $\varphi = \varphi(s, \theta)$, $s \in [0, L]$ and $\theta \in \mathbb{R}$, with

$$\begin{aligned} \varphi_s(s, \theta) &= D\varphi_{\theta\theta}(s, \theta) \quad s \in (0, L], \quad \theta \in \mathbb{R}, \\ \varphi(0, \theta) &= \varphi_0(\theta) \qquad\quad \theta \in \mathbb{R}, \\ \varphi(s, \theta \pm 2\pi) &= \varphi(s, \theta) \qquad s \in [0, L], \quad \theta \in \mathbb{R}. \end{aligned}$$

We assume that φ_0 is periodic with period 2π, and continuous.

For $\nu = 1, 2, 3, 4$, we write

$$\alpha_\nu = \nu\pi/2 - \pi/4 \quad \text{and} \quad \beta_\nu = \nu\pi/2.$$

If $\varphi(\mathrm{s}, \alpha_\nu)$ were given for $s \in [0, L]$, $\nu = 1, 2, 3, 4$, then all of φ could be computed by solving four initial–boundary value problems on the intervals $(-\pi/4, \pi/4)$, $(\pi/4, 3\pi/4)$, $(3\pi/4, 5\pi/4)$, and $(5\pi/4, 7\pi/4)$, with Dirichlet boundary values. Similarly, if $\varphi(s, \beta_\nu)$ were given for $s \in [0, L]$, $\nu = 1, 2, 3, 4$, then all of φ could be computed by solving four similar problems on the intervals $(0, \pi/2)$, $(\pi/2, \pi)$, $(\pi, 3\pi/2)$, and $(3\,\pi/2, 2\,\pi)$. This suggests the following iterative algorithm:

1. Given approximations for $\varphi(s, \alpha_\nu)$, $s \in [0, L]$, $\nu = 1, 2, 3, 4$, compute an approximation for all of φ by solving four separate initial–boundary value problems. In particular, this yields approximations for $\varphi(s, \beta_\nu)$, $s \in [0, L]$, $\nu = 1, 2, 3, 4$.

2. Based on these approximations, compute a new approximation for all of φ, again by solving four separate initial–boundary value problems. In particular, this yields new approximations for $\varphi(s, \alpha_\nu)$, $s \in [0, L]$, $\nu = 1, 2, 3, 4$.

Iterate this process.

We note that in the numerical solution of parabolic problems, domain decomposition is typically used in a different way, namely for the purpose of solving the system of equations resulting from a time-implicit discretization in every time step; see for instance [19, 22]. A method of the kind considered here can only work in very special circumstances, namely when the non-dimensionalized diffusion coefficient is small, and there is no convection in the diffusion direction(s).

We view our method as a fixed point iteration for the quadruple of continuous functions

$$\varphi(s, \alpha_\nu), \quad s \in [0, L], \quad \nu = 1, 2, 3, 4.$$

We denote by V the space of quadruples of continuous functions on $[0, L]$: $V = (C[0, L])^4$, and will analyze the convergence of our method in the *maximum norm* $\|\cdot\|_\infty$ on V: for $\xi = (\xi_1, \xi_2, \xi_3, \xi_4) \in V$,

$$\|\xi\|_\infty = \max_{\nu=1,2,3,4} \max_{s\in[0,L]} |\xi_\nu(s)|.$$

We denote by $\mathscr{L}$ the mapping being iterated. $\mathscr{L}$ maps V into itself, and depends on φ_0. We make this dependence clear in the notation by writing $\mathscr{L}(\varphi_0; \xi)$, $\xi \in V$. $\mathscr{L}(\varphi_0; \xi)$ depends linearly on the pair (φ_0, ξ), so

$$\mathscr{L}(\varphi_0; \xi) = \mathscr{L}(0; \xi) + \mathscr{L}(\varphi_0; 0).$$

This shows that for fixed φ_0, $\mathscr{L}(\varphi_0; \xi)$ acts affine-linearly on ξ. We use the notation $\mathscr{A}\xi = \mathscr{L}(0; \xi)$. The operator norm

$$\|\mathscr{A}\|_\infty = \max_{\xi\in V-\{0\}} \frac{\|\mathscr{A}\xi\|_\infty}{\|\xi\|_\infty}$$

bounds the factor by which each iteration reduces the maximum norm of the error. Using the maximum principle for the heat equation [16, p. 215], $\|\mathscr{A}\|_\infty$ is immediately seen to be bounded by

$$\omega(D, L) = \max_{s\in[0,L]} (\psi(D; s, 0))^2,$$

and $\psi = \psi(D; s, \theta)$ is defined for $D > 0$, $s \geq 0$, and $\theta \in [-\pi/4, \pi/4]$ by

$$\psi_s(D; s, \theta) = D\psi_{\theta\theta}(D; s, \theta) \quad s > 0, \quad \theta \in (-\pi/4, \pi/4), \tag{28}$$

$$\psi(D; 0, \theta) = 0 \quad \theta \in [-\pi/4, \pi/4], \tag{29}$$

$$\psi(D; s, \pm\pi/4) = 1 \quad s > 0. \tag{30}$$

Observing that $\psi(D; s, \theta) = \psi(1; Ds, \theta)$, we see that

$$\omega(D, L) = \max_{s\in[0,L]} (\psi(1; Ds, 0))^2 = \max_{s\in[0,DL]} (\psi(1; s, 0))^2.$$

This shows that ω does not depend on D and L individually, but only on the dimensionless product DL. We shall therefore write $\omega(DL)$ instead of $\omega(D, L)$ from now on.

The analysis of our method for the heat equation is now reduced to analyzing the behavior of the function $\psi_0(s) = \psi(1; s, 0)$, $s \geq 0$. Again using the maximum principle, we see that $\psi_0(s) \in [0, 1)$ for all $s \geq 0$. The initial condition (29) implies $\psi_0(0) = 0$. Equations (28) and (29) imply $\psi_0'(0) = 0$. Differentiating Eq. (28) $l - 1$ times with respect to s, we find that

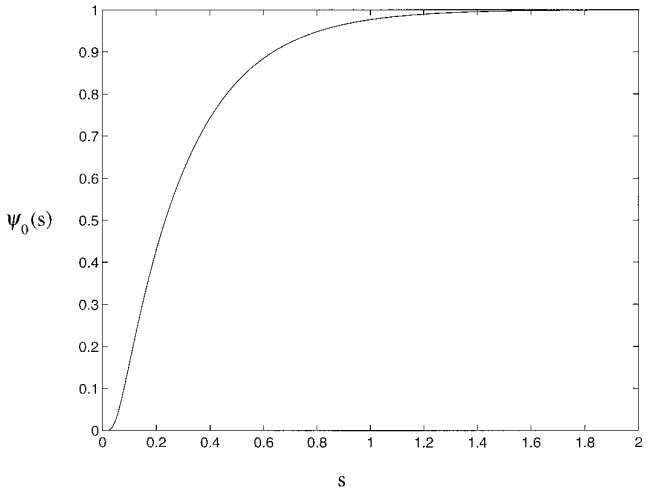

FIG. 6. The graph of the function ψ_0.

$$\frac{\partial^l}{\partial s^l}\psi(D; s, \theta) = D^l \frac{\partial^{2l}}{\partial \theta^{2l}}\psi(D; s, \theta).$$

In combination with Eq. (29), this implies that the lth derivative of ψ_0 at $s = 0$ vanishes. Thus ψ_0 and all its derivatives vanish at $s = 0$, and therefore ψ_0 vanishes to arbitrarily high order as $s \to 0$.

Using Fourier series, we can find an explicit series representation of $\psi_0(s)$. We omit the straightforward computation, and just give its result:

$$\psi_0(s) = 1 \pm \frac{8}{\pi} \sum_{k=0}^{\infty} \frac{(-1)^{k+1}}{4k+2} \exp(-(4k+2)^2 s). \tag{31}$$

Figure 6 shows the graph of ψ_0 as a function of s. This plot was generated using Eq. (31), truncating the sum after 1000 terms; the plot obtained when truncating after 2000 terms is not visibly different. Equation (31) implies that $\lim_{s\to\infty} \psi_0(s) = 1$.

We next sketch a proof that ψ_0 is an increasing function, as suggested by Fig. 6. Observe that $\psi_s(1; s, \theta)$ solves the heat equation. Because of $\psi(1; 0, \theta) \equiv 0$, we have $\psi_s(1; 0, \theta) = \psi_{\theta\theta}(1; 0, \theta) \equiv 0$ for $\theta \in (-\pi/4, \pi/4)$. Because of $\psi(1; s, \pm\pi/4) \equiv 1$, we have $\psi_s(1; s, \pm\pi/4) \equiv 0$ for $s > 0$. The only places in which the initial–boundary data for $\psi_s(1; s, \theta)$ are non-zero are therefore the points $(s, \theta) = (0, \pm\pi/4)$. The data in these points are positive δ-functions. The maximum principle, applied to ψ_s, now implies that $\psi_s(1; \theta, s) > 0$ for $\theta \in (-\pi/4, \pi/4)$ and $s > 0$. It is not difficult to make this argument completely rigorous.

Since ψ_0 is increasing, $\omega(DL) = \psi_0(DL)^2$. Figure 7 shows $\omega(DL)$ as a function of DL. In generating this plot, we again truncated the sum in Eq. (31) after 1000 terms, and

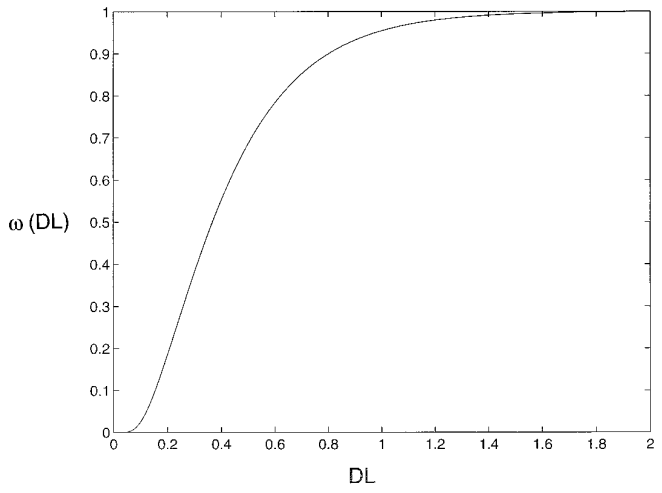

FIG. 7. Theoretical upper bounds on convergence factors for the heat equation.

again the plot obtained when truncating after 2000 terms is not visibly different.

We summarize:

PROPOSITION 3. *The maximum norm convergence factor of the iteration for the heat equation described in this section is bounded by the function*

$$\omega(DL) = \left[1 + \frac{8}{\pi}\sum_{k=0}^{\infty}\frac{(-1)^{k+1}}{4k+2}\exp(-(4k+2)^2\,DL)\right]^2$$

plotted in Fig. 7. This function has the following properties.

(i) $\omega(DL) \in [0, 1)$ *for* $DL \geq 0$,

(ii) $\omega(DL)$ *is an increasing function of* DL,

(iii) *for any* $p > 0$, $\omega(DL) = o((DL)^p)$ *as* $DL \to 0$,

(iv) $\lim_{DL\to\infty} \omega(DL) = 1$.

8. THE ITERATION FOR THE LINEAR BOLTZMANN EQUATION

8.1. *Gauss–Seidel-like version*

We now define an analog of the method of Section 6 for the boundary value problem for the linear Boltzmann equation, Eqs. (6) and (7). The algorithm for the linear Boltzmann equation cannot be stated in precisely the same way as that for the Fokker–Planck equation because Q, unlike Q_{FP}, is not local.

Let again $\hat{I}$ be an open real interval of length smaller than π, and I the corresponding subset of S^1. We denote the complement of I by I^c, and also introduce notation for the subset of $\partial^-\Omega$ corresponding to I:

$$\partial_I^-\Omega = \{(\mathbf{x}, \mathbf{u}) \in \partial\Omega \times \mathrm{I} : \mathbf{u}\cdot\mathbf{n}(\mathbf{x}) < 0\}.$$

If f^{old} is an approximation to f, an improved approximation f^{new} can be obtained by solving

$$uf_x^{\mathrm{new}} + vf_y^{\mathrm{new}} = Qf^{\mathrm{new}} \quad \text{in } \Omega \times I, \tag{32}$$

$$f^{\mathrm{new}} = f^{\mathrm{old}} \quad \text{in } \Omega \times I^c, \tag{33}$$

$$f^{\mathrm{new}} = g \quad \text{in } \partial_I^-\Omega. \tag{34}$$

Equations (32)–(34) can be solved using numerical methods resembling those for initial–boundary value problems for convection–diffusion equations; see Section 10. We write

$$f^{\mathrm{new}} = \mathscr{S}(I, g; f^{\mathrm{old}}).$$

For fixed I, f^{new} depends linearly on g and f^{old}.

In our iterative method, the operator $\mathscr{S}(I, g; \cdot)$ is applied successively with varying choices of I. Specifically, define

$$\hat{I}_\nu = (-\pi/4 + (\nu - 1)\pi/2, -\pi/4 + \nu\pi/2)$$

for $1 \leq \nu \leq 4$, and

$$\hat{I}_\nu = ((\nu - 5)\pi/2, (\nu - 4)\pi/2)$$

for $5 \leq \nu \leq 8$, and denote by I_ν the corresponding subsets of S^1. Starting with an initial guess $f^{(0)}$, our iteration is defined by the recursion formula

$$f^{(k-1+\nu/8)} = \mathscr{S}(I_\nu, g; f^{(k-1+(\nu-1)/8)}) \tag{35}$$

for $k \geq 1$ and $1 \leq \nu \leq 8$.

We note that in this algorithm, the steps must be carried out in sequence. The computation of $f^{(k-1+\nu/8)}$ uses the most recently computed approximations in $\Omega \times I_\nu^c$. This is reminiscent of the Gauss-Seidel method for linear systems, and we therefore call this version of the algorithm "Gauss–Seidel-like."

8.2. *Jacobi-like version*

One of the main motivations for studying domain decomposition methods is their parallelizability. In fact, the method of Section 6 is very easily parallelizable, as was pointed out at the end of Section 6. However, as discussed at the end of Section 8.1, in the Gauss–Seidel-like version of our method for the linear Boltzmann equation, the steps must be carried out in sequence.

Parallelizability can be restored by delaying the use of the computed approximations. This is reminiscent of the Jacobi method for linear systems, and we therefore call

this the "Jacobi-like" version of our algorithm. In this version, Eq. (35) is replaced by

$$f^{(k-1/2)} = \mathscr{S}(I_\nu, g; f^{(k-1)}) \quad \text{in } \Omega \times I_\nu,\ \nu = 1, 2, 3, 4, \quad (36)$$

and

$$f^{(k)} = \mathscr{S}(I_\nu, g; f^{(k-1/2)}) \quad \text{in } \Omega \times I_\nu,\ \nu = 5, 6, 7, 8. \quad (37)$$

9. COMPUTATIONAL RESULTS FOR THE FOKKER–PLANCK EQUATION

9.1. *Discretization*

In our numerical experiments, the spatial domain is the square

$$\Omega = (0, L)^2,$$

with $L > 0$. The iteration in Section 6 involves the solution of a sequence of subproblems in the phase space subdomains $\Omega \times I_\nu$, $1 \le \nu \le 8$. We discretize each of these subproblems separately. The global discretization is defined implicitly only, as the limit computed by the iteration.

We use regular rectangular grids in (x, y, θ)-space, with mesh widths $\Delta s = L/n_s$ in the x- and y-directions, and $\Delta\theta = 2\pi/n_\theta$ in the θ-direction, where n_s and n_θ are positive integers. We assume that n_s is divisible by 4, and n_θ by 8; this is not necessary, but convenient. For integers i, j, and k, we write $x_i = i\Delta s$, $y_j = j\Delta s$, $\theta_k = k\Delta\theta$, $\mathbf{x}_{i,j} = (x_i, y_j)$, and $\mathbf{u}_k = (\cos\theta_k, \sin\theta_k)$.

We begin by describing our discretization of the subproblems in $\Omega \times I_1$. As discussed in Section 6, for $\theta \in (-\pi/4, \pi/4)$, we divide the Fokker–Planck equation by $\cos\theta$, writing it in the form

$$f_x + \tan\theta\, f_y = \frac{D}{\cos\theta} f_{\theta\theta},$$

and think of x as "time." To discretize, we use first order "time" differencing, first order upstream differencing of the convection term (that is, the y-derivative), and second order central differencing of the diffusion term. We treat the convection term explicitly in "time," and the diffusion term implicitly. (For a brief discussion of the reason for treating the diffusion term implicitly, see the end of this section.) Writing $f_{i,j,k}$ for the numerical approximation of $f(x_i, y_j, \theta_k)$, and writing $g_{i,j,k} = g(x_i, y_j, \theta_k)$, where g denotes the boundary data in Eq. (17), our discretization is given by the following formulas, in which we have reversed the division by $\cos\theta$:

For $1 \le i \le n_s$, $0 \le j \le n_s - 1$, and $-n_\theta/8 + 1 \le k \le -1$,

$$\cos\theta_k \frac{f_{i,j,k} - f_{i-1,j,k}}{\Delta s} + \sin\theta_k \frac{f_{i-1,j+1,k} - f_{i-1,j,k}}{\Delta s} = D \frac{f_{i,j,k+1} - 2f_{i,j,k} + f_{i,j,k-1}}{\Delta\theta^2}. \quad (38)$$

For $1 \le i \le n_s$ and $0 \le j \le n_s$,

$$\frac{f_{i,j,0} - f_{i-1,j,0}}{\Delta s} = D \frac{f_{i,j,1} - 2f_{i,j,0} + f_{i,j,-1}}{\Delta\theta^2}. \quad (39)$$

For $1 \le i \le n_s$, $1 \le j \le n_s$, and $1 \le k \le n_\theta/8 - 1$,

$$\cos\theta_k \frac{f_{i,j,k} - f_{i-1,j,k}}{\Delta s} + \sin\theta_k \frac{f_{i-1,j,k} - f_{i-1,j-1,k}}{\Delta s} = D \frac{f_{i,j,k+1} - 2f_{i,j,k} + f_{i,j,k-1}}{\Delta\theta^2}. \quad (40)$$

For $0 \le i, j \le n_s$ and $-n_\theta/8 + 1 \le k \le n_\theta/8 - 1$ with $(\mathbf{x}_{i,j}, \mathbf{u}_k) \in \partial^- \Omega$,

$$f_{i,j,k} = g_{i,j,k}. \quad (41)$$

For $0 \le i, j \le n_s$,

$$f_{i,j,-n_\theta/8} \text{ and } f_{i,j,n_\theta/8} \text{ given from a previous iteration or initial guess.} \quad (42)$$

Equations (38)–(42) are solved by marching in the direction of increasing i, solving a positive definite, symmetric, tridiagonal system of linear equations for each spatial grid point $\mathbf{x}_{i,j}$ with $1 \le i \le n_s$, $0 \le j \le n_s$.

The discretization of the subproblems in $\Omega \times I_\nu$ for $\nu = 2, 3, 4$ is exactly analogous.

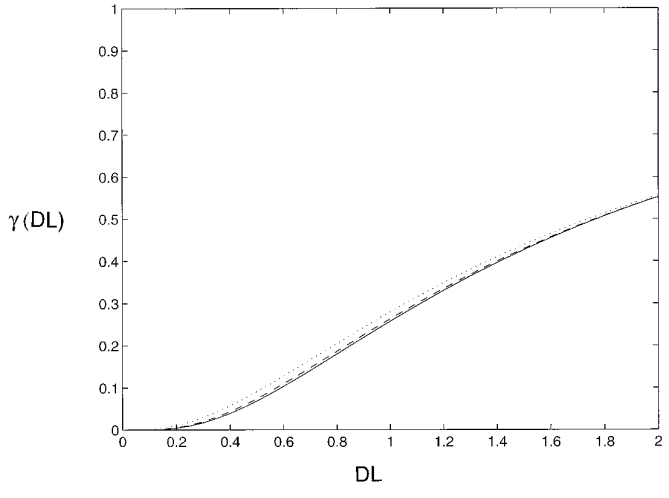

FIG. 8. Experimentally determined convergence factors for the Fokker–Planck equation.

TABLE II

Observed Convergence Factors of the Iteration for the Fokker–Planck Equation in $(0, L)^2 \times S^1$, as a Function of DL

DL	0.05	0.1	0.2	0.5	1.0	2.0
γ	0.43×10^{-6}	0.11×10^{-3}	0.40×10^{-2}	0.69×10^{-1}	0.26×10^{0}	0.55×10^{0}

In $\Omega \times I_5$, we use upstream first order differencing for the x- and y-derivatives, and central second order differencing for the diffusion term:

For $1 \le i, j \le n_s$, $1 \le k \le n_\theta/4 - 1$,

$$\cos\theta_k \frac{f_{i,j,k} - f_{i-1,j,k}}{\Delta s} + \sin\theta_k \frac{f_{i,j,k} - f_{i,j-1,k}}{\Delta s} = D \frac{f_{i,j,k+1} - 2f_{i,j,k} + f_{i,j,k-1}}{\Delta\theta^2}. \tag{43}$$

For $i = 0$ or $j = 0$ and $1 \le k \le n_\theta/4 - 1$,

$$f_{i,j,k} = g_{i,j,k}. \tag{44}$$

For $0 \le i, j \le n_s$,

$$f_{i,j,0} \text{ and } f_{i,j,n_\theta/4} \text{ given from a previous iteration or initial guess.} \tag{45}$$

Equations (43)–(45) are solved by marching in the direction of increasing $i + j$, solving a positive definite, symmetric, tridiagonal system of linear equations for each spatial grid point $\mathbf{x}_{i,j}$ with $1 \le i, j \le n_s$.

The discretization of the subproblems in $\Omega \times I_\nu$ for $\nu = 6, 7, 8$ is exactly analogous.

Recalling $\Delta s = L/n_s$, we see that Eqs. (38)–(42) and (43)–(45) do not depend on D and L individually, but only on the dimensionless product DL. This completes the description of our difference scheme. It is one of the simplest possible discretizations, and of low accuracy. However, since we have described our iteration without reference to any discretization in Section 6, we expect that it could be implemented in conjunction with much more sophisticated discretization schemes.

Our "time"-implicit treatment of the diffusion term in each subdomain $\Omega \times I_\nu$ avoids the parabolic stability constraint. More importantly, it also avoids accuracy problems caused by the fact that the inflow boundary data are δ-functions with respect to direction for mono-directionally incident beams, which are of particular interest to us. We intend to return to this point in much greater detail in future work. We note that the similar issue of how to numerically handle singular initial data for parabolic partial differential equations has been studied extensively. For instance, for a convergence result for finite element discretizations of parabolic initial–boundary value problems allowing δ-function initial data, see [4].

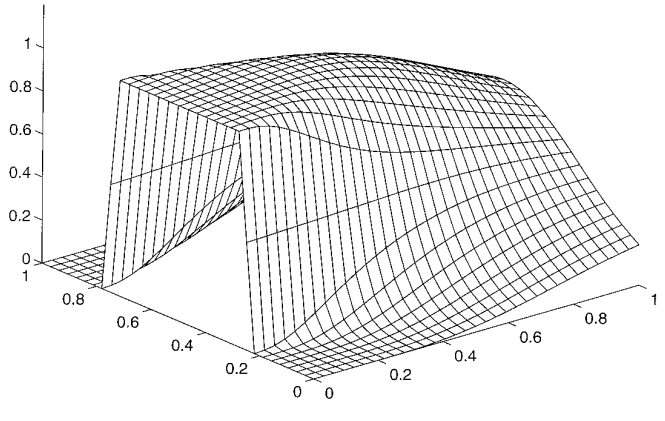

FIG. 9. Macroscopic density of a broad, mono-directional beam, Fokker–Planck equation, $D = 0.1$.

9.2. *Convergence Speed of the Iteration*

To test the convergence speed of our method, we consider Eqs. (16) and (17) with $g \equiv 0$, so that the solution is $f \equiv 0$, and start the iteration with the initial guess

$$f^{(0)}_{i,j,k} = \begin{cases} 1 & \text{for } 1 \le i, j \le n_s - 1, \quad 0 \le k \le n_\theta \\ 0 & \text{for } i \in \{0, n_s\} \text{ or } j \in \{0, n_s\}, \quad 0 \le k \le n_\theta. \end{cases}$$

In general, the choice of data and initial guess is not very important in testing the speed of convergence of a linear iteration for a system of linear equations. Taking the solution of the test problem to be zero has the advantage that the influence of the finite machine precision interferes with the computation only after a very large number of iterations, namely when the computed approximations become as small as the smallest positive machine number. By contrast, for a test problem with a non-zero solution, round-off errors become significant much earlier, namely when the relative discrepancy between the computed approximation and the exact solution comes close to the machine epsilon.

We denote by γ an approximation for the spectral radius of the iteration matrix of our method. We describe the precise algorithm used to compute γ in the next paragraph.

We begin by taking five preliminary iterations in order to give the most slowly convergent error components time to become dominant. We then take the geometric average of the convergence factors over m further iterations, with m determined as follows. We begin with $m = 5$. We then double m, and compare the two averages obtained. If they differ by less than one percent, we let γ be the average obtained with the larger number of iterations; otherwise we double m again, continuing in this way until the discrepancy between two consecutive approximations is less than one percent, or m becomes 80. It is rare that the algorithm halts because m has become equal to 80; even then, the discrepancy between the last two computed average convergence factors is never greater than 10%. Thus γ can be expected to be a reasonably good approximation of the spectral radius of the iteration matrix of our method.

The value of γ depends on the grid and on DL. Figure 8 shows γ, as a function of DL, computed on grids with $16 \times 16 \times 16$ (dots), $32 \times 32 \times 32$ (dashes), and $64 \times 64 \times 64$ mesh cells (solid). Notice that γ is nearly grid independent, and in fact decreases slightly as the grid is refined. Notice also that Fig. 8 is qualitatively similar to Fig. 7. Quantitative agreement cannot be expected, since Fig. 7 shows upper bounds (and certainly not sharp ones) for convergence factors for the heat equation, while Fig. 8 shows actual convergence factors for the Fokker–Planck equation.

Table II shows some of the numbers that Fig. 8 is based on, for the $64 \times 64 \times 64$ grid.

9.3. *Example of a Computed Beam*

For illustration, we present a picture of a computed beam. We take $L = 1$ and consider a broad, normally incident beam, corresponding to the inflow boundary data

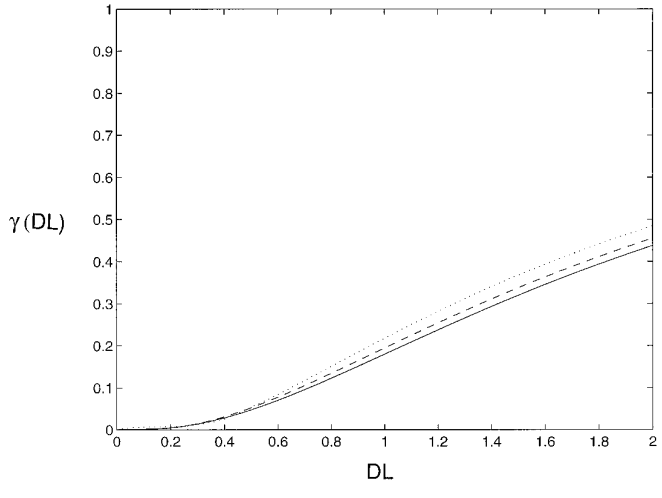

FIG. 10. Experimentally determined convergence factors for the linear Boltzmann equation with screened Rutherford scattering: Gauss–Seidel-like version.

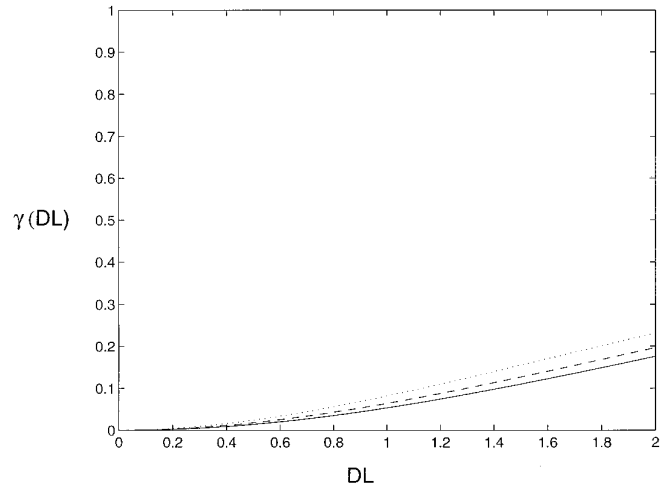

FIG. 11. Experimentally determined convergence factors for the linear Boltzmann equation with Henyey–Greenstein scattering: Gauss–Seidel-like version.

$$g(\mathbf{x}, \mathbf{u}) = \begin{cases} \delta_{\mathbf{e}_1}(\mathbf{u}) & \text{if } x = 0,\ 1/4 \le y \le 3/4, \\ 0 & \text{otherwise,} \end{cases}$$

where $\mathbf{e}_1 = (1, 0) \in S^1$, and $\delta_{\mathbf{e}_1}$ denotes the Dirac δ-function on S^1 centered at $\mathbf{e}_1$. We discretize these inflow data as follows:

$$g_{i,j,k} = \begin{cases} n_\theta/(2\pi) & \text{if } i = 0,\ n_s/4 + 1 \le j \le 3n_s/4 - 1,\ k = 0 \bmod n_\theta, \\ n_\theta/(4\pi) & \text{if } i = 0,\ j = n_s/4 \text{ or } j = 3n_s/4,\ k = 0 \bmod n_\theta, \\ 0 & \text{otherwise.} \end{cases}$$

For $D = 0.1$, Fig. 9 shows the computed approximation of the *macroscopic density*

$$\int_0^{2\pi} f(\mathbf{x}, \theta)\, d\theta \tag{46}$$

as a function of $\mathbf{x}$. These computations were carried out on a $64 \times 64 \times 64$ grid, and the integral in (46) was approximated using the trapezoid method. The figure shows the result of three iterations starting from a zero initial guess, plotted on a 32×32 spatial mesh. Further iterations would not lead to any visible change in the figure.

10. COMPUTATIONAL RESULTS FOR THE LINEAR BOLTZMANN EQUATION

10.1. *Discretization*

Equation (5) is the basis for our discretization of the collision operator:

TABLE III

Observed Convergence Factors of the Iteration for the Linear Boltzmann Equation with Screened Rutherford Scattering in $(0, L)^2 \times S^1$ with $\overline{\lambda}/L = 1/20{,}000$, as a Function of DL

DL	0.05	0.1	0.2	0.5	1.0	2.0
γ	0.27×10^{-3}	0.64×10^{-3}	0.49×10^{-2}	0.47×10^{-1}	0.18×10^{0}	0.44×10^{0}

$$Qf(\theta) = \frac{1}{\overline{\lambda}}(p * f - f)(\theta) = \sum_n \frac{c_n - 1}{\overline{\lambda}} \hat{f}_n \exp(in\theta).$$

We use a pseudo-spectral discretization, obtained by restricting the summation to $-n_\theta/2 \le n \le n_\theta/2 - 1$, restricting θ to values of the form $\theta_k = k\Delta\theta$, k integer, and re-interpreting $\hat{f}_n$ as the nth discrete Fourier coefficient on the grid

$$\{k\Delta\theta : -n_\theta/2 \le k \le n_\theta/2 - 1\}.$$

More explicitly, the discretization of Q is a linear operator Q_{n_θ} mapping the space of 2π-periodic functions defined on the grid

$$\{\theta_k = k\Delta\theta : k \text{ integer}\}$$

into itself. Identifying such a function with the vector $\mathbf{f} = (f_k)_{-n_\theta/2 \le k \le n_\theta/2-1}$ of its values in the grid points $\theta_k = k\Delta\theta$, $-n_\theta/2 \le k \le n_\theta/2 - 1$, we can also think of Q_{n_θ} as an $n_\theta \times n_\theta$ matrix, defined as follows:

$$(Q_{n_\theta}\mathbf{f})_k = \sum_{n=-n_\theta/2}^{n_\theta/2-1} \frac{c_n - 1}{\overline{\lambda}} \left(\frac{1}{n_\theta} \sum_{l=-n_\theta/2}^{n_\theta/2-1} \exp(-in\theta_l) f_l \right) \exp(in\theta_k).$$

Using $c_n = c_{-n}$, we see that

$$(Q_{n_\theta}\mathbf{f})_k = \frac{1}{n_\theta} \sum_{n=-n_\theta/2}^{n_\theta/2-1} \sum_{l=-n_\theta/2}^{n_\theta/2-1} \frac{c_n - 1}{\overline{\lambda}} \cos(n(\theta_k - \theta_l)) f_l,$$

which shows that Q_{n_θ} is real and symmetric. Elementary facts from discrete Fourier analysis imply that the vectors

$$\mathbf{f}_m = (\exp(im\theta_l))_{-n_\theta/2 \le l \le n_\theta/2-1},$$

$-n_\theta/2 \le m \le n_\theta/2 - 1$, are linearly independent eigenvectors of Q_{n_θ}, with eigenvalues $(c_m - 1)/\overline{\lambda}$. Since $c_0 = 1$ and $c_m < 1$ for $m \ne 0$, we obtain:

PROPOSITION 4. *The matrix $Q_{n_\theta} \in \mathbb{R}^{n_\theta \times n_\theta}$ is symmetric and negative semidefinite, with eigenvalues $(c_m - 1)/\overline{\lambda}$, $-n_\theta/2 \le m \le n_\theta/2 - 1$. The kernel of Q_{n_θ} is one-dimensional, spanned by the vector $(1, 1, ..., 1)^T \in \mathbb{R}^{n_\theta}$.*

The discretization of the subproblems for the linear Boltzmann equation is exactly the same as in Section 9.1, except that the three-point discretization of Q_{FP} is replaced by the discretization of Q described in the preceding paragraph. As before, the subproblems are solved by marching, and this involves solving a system of linear equations for each spatial gridpoint. These systems are symmetric and positive definite because of Proposition 4. As a result of the global nature of Q and its discretization, they are dense, and thus the method is substantially more expensive than that of Section 9. However, an increased expense is unavoidable unless one is willing to approximate Q by a local operator.

10.2. *Convergence Speed of the Gauss–Seidel-like Version*

In this section, we present numerical results for the linear Boltzmann equation with our planar versions of screened Rutherford and Henyey–Greenstein scattering; see Eqs. (21) and (22). Once the form of p (for instance, Eq. (21) or Eq. (22)) has been chosen, there are two parameters to be selected, $\overline{\lambda}$ and ε. Alternatively, we may select the dimensionless parameters $\overline{\lambda}/L$ and DL, where D is defined as before by Eq. (8). In our test code, the parameter ε of Section 4 is then computed numerically, by solving the equation

TABLE IV

Observed Convergence Factors of the Iteration for the Linear Boltzmann Equation with Henyey–Greenstein Scattering in $(0, L)^2 \times S^1$ with $\overline{\lambda}/L = 1/20{,}000$, as a Function of DL

DL	0.05	0.1	0.2	0.5	1.0	2.0
γ	0.18×10^{-3}	0.63×10^{-3}	0.24×10^{-2}	0.14×10^{-1}	0.53×10^{-1}	0.18×10^{0}

TABLE V

Observed Convergence Factors of the Iteration for the Linear Boltzmann Equation with Screened Rutherford Scattering in $(0, L)^2 \times S^1$ with $DL = 0.1$, as a Function of $\bar{\lambda}/L$

$\bar{\lambda}/L$	1/100	1/1,000	1/10,000	1/100,000
γ	0.77×10^{-3}	0.72×10^{-3}	0.66×10^{-3}	0.62×10^{-3}

$$\frac{1}{2\bar{\lambda}/L}\int_{-\pi}^{\pi} \eta^2 p(\varepsilon; \eta)\, d\eta = DL$$

for ε, using the bisection method. After ε has been determined, the Fourier coefficients c_n are evaluated by numerical quadrature. All of these computations are carried out with at least 10-digit accuracy.

As in Section 9, the discretized problem depends on n_s, n_θ, and DL; in addition, it now also depends on $\bar{\lambda}/L$.

To test the convergence speed of the Gauss–Seidel-like version of our iteration, we proceed as in Section 9.2. In analogy with Fig. 8, Fig. 10 shows our estimate γ for the spectral radius of the iteration matrix as a function of DL for screened Rutherford scattering with $\bar{\lambda}/L = 1/20{,}000$. Figure 11 shows the same for Henyey–Greenstein scattering. As before, the three lines correspond to three different grid sizes: $16 \times 16 \times 16$ (dotted), $32 \times 32 \times 32$ (dashed), and $64 \times 64 \times 64$ (solid). Comparing Figs. 8, 10, and 11, we see that except for the smallest values of DL, convergence is slightly faster for screened Rutherford scattering, and significantly faster for Henyey–Greenstein scattering. This is not surprising for the following reason. In comparison with the Fokker–Planck equation, beam broadening is somewhat less pronounced for screened Rutherford scattering (see [2]), much less pronounced for Henyey–Greenstein scattering (see Fig. 15 below), and the analysis of Section 7 suggests that less beam broadening should result in faster convergence of our iteration.

Tables III and IV show some of the numbers that Figs. 10 and 11 are based on, for the $64 \times 64 \times 64$ grid. Tables V and VI similarly show γ as a function of $\bar{\lambda}/L$, with $DL = 0.1$ fixed; again the computations were carried out on the $64 \times 64 \times 64$ grid. It appears that γ does not strongly depend on the value of $\bar{\lambda}/L$.

TABLE VI

Observed Convergence Factors of the Iteration for the Linear Boltzmann Equation with Henyey–Greenstein Scattering in $(0, L)^2 \times S^1$ with $DL = 0.1$, as a Function of $\bar{\lambda}/L$

$\bar{\lambda}/L$	1/100	1/1,000	1/10,000	1/100,000
γ	0.63×10^{-3}	0.63×10^{-3}	0.63×10^{-3}	0.63×10^{-3}

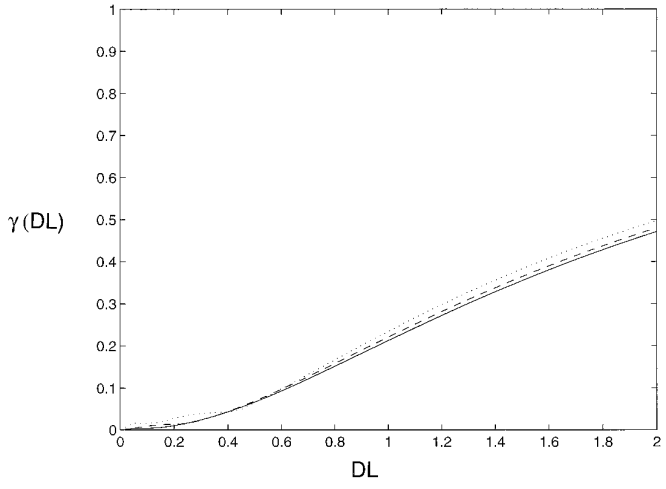

FIG. 12. Experimentally determined convergence factors for the linear Boltzmann equation with screened Rutherford scattering: Jacobi-like version.

10.3. *Convergence Speed of the Jacobi-Like Version*

In analogy with Figs. 10 and 11, Figs. 12 and 13 show the spectral radius of the iteration matrix as a function of DL, for screened Rutherford and Henyey–Greenstein scattering, using the Jacobi-like version of our iteration. As before, the three lines correspond to three different grid sizes: $16 \times 16 \times 16$ (dotted), $32 \times 32 \times 32$ (dashed), and $64 \times 64 \times 64$ (solid). Comparing Figs. 12 and 13 with Figs. 10 and 11, we see that convergence is, as one should expect, somewhat slower for the Jacobi-like version than for the Gauss–Seidel-like version. However, the difference is surprisingly small.

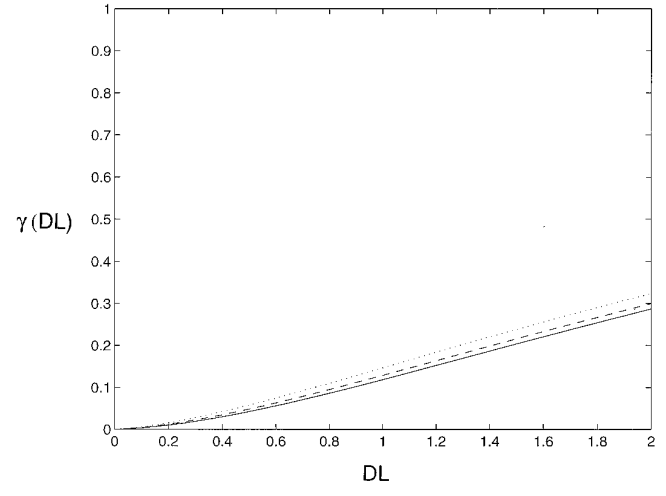

FIG. 13. Experimentally determined convergence factors for the linear Boltzmann equation with Henyey–Greenstein scattering: Jacobi-like version.

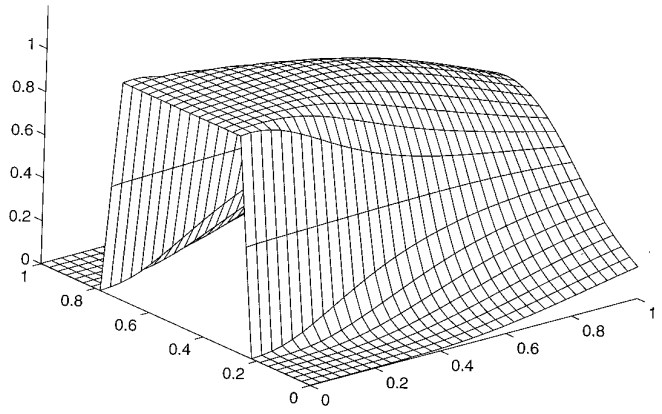

FIG. 14. Macroscopic density of a broad, mono-directional beam, linear Boltzmann equation, screened Rutherford scattering, $D = 0.1$.

10.4. *Examples of Computed Beams*

We again present pictures of computed beams for illustration. Figure 14 shows the analog of Fig. 9 for screened Rutherford scattering, with $\overline{\lambda}/L = 1/20{,}000$. Figure 15 shows the same for Henyey–Greenstein scattering. Each of these was computed using three iterations of the Gauss–Seidel-like version of our algorithm, starting with a zero initial guess. Further iterations do not visibly change these figures. As expected, Fig. 14 is similar to Fig. 9, while Fig. 15 is completely different, illustrating the incorrectness of the Fokker–Planck approximation for Henyey–Greenstein scattering.

11. SUMMARY AND DISCUSSION

For mono-energetic, two-dimensional linear particle beam problems discretized on a grid, we have shown that angular domain decomposition yields a very fast iterative solver. We obtain rapid convergence as long as the non-dimensionalized angular diffusion coefficient DL is at most of moderate size.

In three space dimensions, there is no precise analog of the method of Section 6, not even for the Fokker–Planck equation. The reason is that the boundaries of two overlapping domains in S^2 that are topologically equivalent to disks and not contained in each other must intersect each other. However, there appears to be no obstacle to formulating an algorithm as in Section 8 for three-dimensional and energy-dependent problems.

Attractive features of the angular domain decomposition method are its conceptual simplicity and easy parallelizability. However, it does become slow when DL becomes large.

The angular domain decomposition method is a cousin of the *angular multigrid* method, which has been proposed and shown to be highly efficient, at least in one space dimension, in [25]. This idea ought to generalize to higher-dimensional problems as well. At this point we do not have enough experience with the two approaches to give a discussion of when to use which, or how they might be combined.

Electron beam therapy planning has been the motivating example in this paper. However, the methods currently used in radiotherapy planning are quite different from the ones studied in this paper. The main class of methods used in electron beam therapy planning is the *pencil beam algorithms* [14]. These are based on approximate closed-form descriptions of beams, obtained experimentally or analytically.

A widely recognized difficulty with pencil beam algorithms stems from the fact that the approximation formulas they rely on are typically derived for spatially homogeneous materials. It is hard to achieve good accuracy with such algorithms in the presence of air pockets, for example. There are two ways of trying to overcome this difficulty. The first is to take background inhomogeneities into account in the analytically derived closed-form descriptions of beams; see, for example, [13, 15]. The second is to use closed-form descriptions of beams penetrating homogeneous backgrounds locally only; methods of this nature are the *pencil beam redefinition algorithms* (see [31, 32]) and, more recently, the *phase space evolution methods* (see for instance [11]). The latter closely resemble grid-based algorithms for the linear Boltzmann equation, although the linear Boltzmann equation is not usually written down explicitly in derivations of the methods. The angular domain decomposition method can be viewed as a variation on these methods in which a few iterations are performed with the aim of accurately solving the discretized linear Boltzmann equation.

The discretization schemes used in this paper are simple and leave much to be desired. However, since our iterative

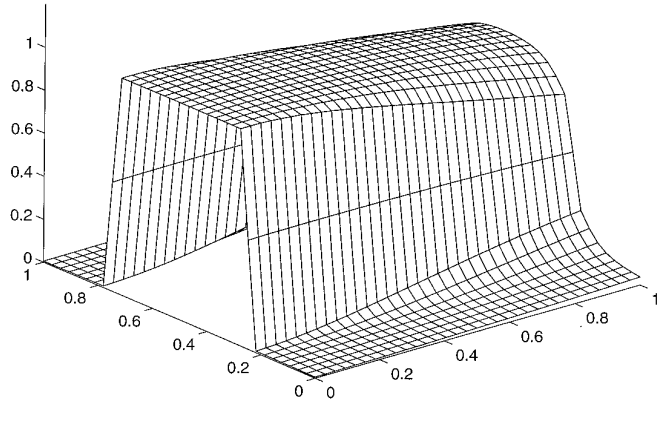

FIG. 15. Macroscopic density of a broad, mono-directional beam, linear Boltzmann equation, Henyey–Greenstein scattering, $D = 0.1$.

method can be described without reference to any discretization at all, we expect that it can be used in conjunction with many discretization schemes. The discretization of the linear Boltzmann equation in the case of forward-peaked scattering has been studied extensively in the nuclear engineering literature; see for example [3, 7, 8, 20, 23, 24].

The choice of the decompositions of the set of particle directions in this paper is the simplest and most symmetric, not necessarily the most efficient one. In fact, the analysis of Section 7 suggests that larger intervals $\hat{I}$ should result in faster convergence. If S^1 were decomposed into only two pieces, the expression by which the equation is divided when it is reformulated as a ''time''-dependent convection–diffusion equation would vanish at the boundary of I. This would lead to difficulties; for instance, for a discretization of the sort we have used in this paper, the hyperbolic stability constraint would become infinitely severe, i.e. impossible to satisfy. However, decompositions of S^1 into three pieces instead of four may lead to even faster convergence than we have obtained.

Improvements and extensions of the method along the indicated lines will be the subject of future work.

ACKNOWLEDGMENT

The author is supported in part by NSF Grant DMS-9626696.

REFERENCES

1. C. Börgers and E. W. Larsen, *Nucl. Sci. Eng.* **123,** 343 (1996).
2. C. Börgers and E. W. Larsen, *Med. Phys.* **23,** 1749 (1996).
3. M. Caro and J. Ligou, *Nucl. Sci. Eng.* **83,** 242 (1983).
4. M. Crouzeix, S. Larsson, and V. Thomée, *Math. Comput.* **63,** No. 207, 121 (1994).
5. J. J. Duderstadt, *Nuclear Reactor Analysis* (Wiley, New York, 1976).
6. J. J. Duderstadt and W. R. Martin, *Transport Theory* (Wiley, New York, 1979).
7. W. L. Filippone, The theory and applicaton of SMART electron scattering matrices, *Nucl. Sci. Eng.* **99,** 232 (1988).
8. W. L. Filippone, J. E. Morel, and W. F. Walters, An extended first collision source method for electron beam source problems, *Nucl. Sci. Eng.* **112,** 1 (1992).
9. L. G. Henyey and J. L. Greenstein, Diffuse radiation in the galaxy, *Astrophys. J.* **93,** 70 (1941).
10. International Commission on Radiation Units and Measurement, *Radiation Dosimetry: Electron Beams with Energies between 1 and 50 MeV*, Report 35 (Bethesda, MD, 1984).
11. J. J. Janssen, D. E. J. Riedeman, M. Morawska-Kaczyńska, P. R. M. Storchi, and H. Huizenga, *Phys. Med. Biol.* **39,** 1351 (1994).
12. D. Jette, *Med. Phys.* **15,** 123 (1988).
13. D. Jette, *Med. Phys.* **18,** 123 (1991).
14. D. Jette, in *Radiation Therapy Physics*, edited by A. R. Smith (Springer-Verlag, Berlin, 1995), p. 95.
15. D. Jette and S. Walker, *Med. Phys.* **19,** 1241 (1991).
16. F. John, *Partial Differential Equations*, 4th ed. (Springer-Verlag, New York, 1982).
17. S. C. Klevenhagen, *Physics and Dosimetry of Therapy Electron Beams* (Medical Physics Publishing, Madison, WI, 1993).
18. D. E. Keyes and J. Xu (Eds.), *Proceedings of the Seventh International Conference on Domain Decomposition, October 27–30, 1993, The Pennsylvania State University,* published as *Contemp. Math.* **180** (1994).
19. Y. A. Kuznetsov, Overlapping domain decomposition methods for parabolic problems, in [28], p. 63.
20. M. Landesman and J. E. Morel, *Nucl. Sci. Eng.* **103,** 1 (1989).
21. E. W. Larsen, Abstract #L23, *Med. Phys.* **20,** 887 (1993).
22. T. P. Mathew, P. L. Polyakov, G. Russo, and J. Wang, *SIAM J. Sci. Comput.*, in press.
23. J. E. Morel, *Nucl. Sci. Eng.* **89,** 131 (1985).
24. J. E. Morel, *Nucl. Sci. Eng.* **101,** 72 (1989).
25. J. E. Morel and T. A. Manteuffel, *Nucl. Sci. Eng.* **107,** 330 (1991).
26. S. T. Perkins, D. E. Cullen, and S. M. Seltzer, *Tables and Graphs of Electron-Interaction Cross Sections from 10 eV to 100 GeV Derived from the LLNL Evaluated Electron Data Library (EEDL) Z = 1–100* (Lawrence Livermore National Laboratory, 1991).
27. G. C. Pomraning, *Math. Mod. Methods Appl. Sci.* **2,** No. 1, 21 (1992).
28. A. Quarteroni, J. Periaux, Y. A. Kuznetsov, and O. B. Widlund (eds.), *Proceedings of the Sixth International Conference on Domain Decomposition, June 15–19, 1992, Como (Italy),* published as *Contemp. Math.* **157** (1994).
29. L. Reimer, *Scanning Electron Microscopy* (Springer-Verlag, Berlin, 1985).
30. B. Rossi and K. Greisen, *Rev. Mod. Phys.* **13,** 240 (1941).
31. A. S. Shiu and K. R. Hogstrom, *Med. Phys.* **18,** 7 (1991).
32. P. R. M. Storchi and H. Huizenga, On a numerical approach of the pencil beam model, *Phys. Med. Bio.* **30,** No. 5, 467 (1985).
33. C. D. Zerby and F. L. Keller, Electron transport theory, calculations, and experiments, *Nucl. Sci. Eng.* **27,** 190 (1967).
34. J. F. Ziegler, J. P. Biersack, and J. Littmart, *The Stopping Power and Range of Ions in Solids* (Pergamon, New York, 1985).